Brain, Behavior, and Immunity 44 (2015) 82–90

Contents lists available at ScienceDirect

Brain, Behavior, and Immunity

journal homepage: www.elsevier.com/locate/ybrbi

# Early postnatal respiratory viral infection alters hippocampal neurogenesis, cell fate, and neuron morphology in the neonatal piglet

Matthew S. Conrad [a,b,c], Samantha Harasim [d], Justin S. Rhodes [b,e], William G. Van Alstine [f], Rodney W. Johnson [a,b,c,g,*]

[a] Department of Animal Sciences, University of Illinois at Urbana–Champaign, Urbana, IL, USA
[b] Neuroscience Program, University of Illinois at Urbana–Champaign, Urbana, IL, USA
[c] Integrative Immunology and Behavior Program, University of Illinois at Urbana–Champaign, Urbana, IL, USA
[d] Department of Molecular and Cellular Biology, University of Illinois at Urbana–Champaign, Urbana, IL, USA
[e] Department of Psychology, University of Illinois at Urbana–Champaign, Urbana, IL, USA
[f] Department of Comparative Pathobiology, Purdue University, West Lafayette, IN 47907, USA
[g] Division of Nutritional Sciences, University of Illinois at Urbana–Champaign, Urbana, IL, USA

ARTICLE INFO

*Article history:*
Received 21 July 2014
Received in revised form 18 August 2014
Accepted 18 August 2014
Available online 28 August 2014

*Keywords:*
Infection
Neurogenesis
Neuron morphology
Inflammation
Piglet

ABSTRACT

Respiratory viral infections are common during the neonatal period in humans, but little is known about how early-life infection impacts brain development. The current study used a neonatal piglet model as piglets have a gyrencephalic brain with growth and development similar to human infants. Piglets were inoculated with porcine reproductive and respiratory syndrome virus (PRRSV) to evaluate how chronic neuroinflammation affects hippocampal neurogenesis and neuron morphology. Piglets in the neurogenesis study received one bromodeoxyuridine injection on postnatal day (PD) 7 and then were inoculated with PRRSV. Piglets were sacrificed at PD 28 and the number of BrdU+ cells and cell fate were quantified in the dentate gyrus. PRRSV piglets showed a 24% reduction in the number of newly divided cells forming neurons. Approximately 15% of newly divided cells formed microglia, but this was not affected by sex or PRRSV. Additionally, there was a sexual dimorphism of new cell survival in the dentate gyrus where males had more cells than females, and PRRSV infection caused a decreased survival in males only. Golgi impregnation was used to characterize dentate granule cell morphology. Sholl analysis revealed that PRRSV caused a change in inner granule cell morphology where the first branch point was extended further from the cell body. Males had more complex dendritic arbors than females in the outer granule cell layer, but this was not affected by PRRSV. There were no changes to dendritic spine density or morphology distribution. These findings suggest that early-life viral infection can impact brain development.


## 1. Introduction

Respiratory infections are common in neonates, but little is known about their impact on short- and long-term brain development (Hall et al., 2009). This is important because brain development in the neonatal period is characterized by extensive dendritic growth, synaptogenesis, gliogenesis, and myelination (Dietrich et al., 1988; Huttenlocher, 1979; Rice and Barone, 2000). Furthermore, although neurogenesis occurs primarily during the prenatal period, the subependymal of the lateral ventricles and hippocampal dentate gyrus are two regions where neurogenesis continues into adulthood (Ekdahl, 2012). During infection, immune-to-brain signaling pathways activate brain microglia, causing increased production of pro-inflammatory cytokines (Dantzer and Kelley, 2007). Developing and mature neurons and glia have numerous pro-inflammatory cytokine receptors and are sensitive to inflammatory conditions (Dantzer and Kelley, 2007). Therefore, understanding the impact of early-life infection on brain development is crucial. A number of psychiatric disorders are associated with neuroimmune alterations and are thought to have developmental origins (Boksa, 2010; Meyer et al., 2011).

Studies in adult animals suggest infection-related neuroinflammation inhibits neurogenesis and alters neuron morphology. One brain area that is especially vulnerable to inflammation and is important for spatial learning and memory is the hippocampus (Elmore et al., 2012). Peripheral immune activation with

* Corresponding author at: 227 Edward R. Madigan Laboratory, 1201 West Gregory Drive, Urbana, IL 61801, USA. Tel.: +1 (217) 333 2118; fax: +1 (217) 333 7861.
*E-mail addresses:* mconra3@illinois.edu (M.S. Conrad), rwjohn@illinois.edu (R.W. Johnson).

http://dx.doi.org/10.1016/j.bbi.2014.08.009
0889-1591/

lipopolysaccharide (LPS) increased the expression of pro-inflammatory cytokines in the brain (Kelley et al., 2003) and inhibited the survival of newborn neurons in the dentate gyrus without impacting cell proliferation (Ekdahl et al., 2003). Pro-inflammatory cytokines also affect neural precursor generation, differentiation, and survival (Cacci et al., 2008; Vallieres et al., 2002; Wu et al., 2012, 2013).

Pro-inflammatory cytokines can further impair synaptic plasticity by inhibiting production of neurotrophins like BDNF, inhibiting long-term potentiation, and altering the architecture of dendrites (Jurgens et al., 2012; Lynch, 2002; Milatovic et al., 2003; Richwine et al., 2008; Tong et al., 2008). Although these and many other studies show that infection and neuroinflammation inhibits neurogenesis and alters neuron morphology in the adult brain, there has been little research on how infection affects neurogenesis or neuron morphology in the critical early postnatal period (Green and Nolan, 2014).

Therefore, the goal of this study was to determine the impact of respiratory viral infection in the early postnatal period on hippocampal neurogenesis, cell fate, and neuron morphology in a domestic piglet model. The piglet is a good model for this type of investigation because it has a gyrencephalic brain that grows and develops similar to human infants (Conrad et al., 2012). In the present study, piglets were experimentally infected on postnatal day (PD) 7 with porcine reproductive and respiratory syndrome virus (PRRSV) and neurogenesis and neuron morphology were determined with brain tissue collected PD 28. PRRSV activates microglia in the hippocampus of piglets and causes increased pro-inflammatory cytokine production and deficits in hippocampal-dependent learning and memory (Elmore et al., 2014). Here we show that PRRSV infection impacts new cell survival, cell fate, and granule cell morphology. These findings are the first to show that a respiratory viral infection in the neonatal period alters neurogenesis and neuron morphology.

## 2. Materials and methods

### 2.1. Animals, housing, and feeding

Naturally farrowed crossbred piglets from six separate litters (20 males and 20 females) were obtained from the University of Illinois swine herd. Piglets were brought to the biomedical animal facility on PD 2 (to allow for colostrum consumption from the sow) and placed in individual cages (0.76 m $L \times 0.58$ m $W \times 0.47$ m $H$) designed for neonatal piglets (Elmore et al., 2014). Each cage was positioned in a rack, with stainless steel perforated side walls and clear acrylic front and rear doors within one of two separate but identical disease containment chambers that have been described (Elmore et al., 2014). Each cage was fitted with flooring designed for neonatal animals (Tenderfoot/NSR, Tandem Products, Inc., Minneapolis, MN, USA). A toy (plastic Jingle Ball™, Bio-Serv, Frenchtown, NJ, USA) was provided to each piglet. Room temperature was maintained at 27 °C and each cage was equipped with an electric heat pad (K&H Lectro-Kennel™ Heat Pad, K&H Manufacturing, LLC, Colorado Springs, CO, USA). Piglets were maintained on a 12-h light/dark cycle; however, during the dark cycle minimal lighting was provided.

Piglets were fed a commercial sow milk replacer (Advance Liqui-Wean, Milk Specialties Co., Dundee, IL, USA). Milk was reconstituted daily to a final concentration of 206 g/L using tap water and supplied at a rate of 285 mL/kg BW (based on daily recorded weights) to a stainless steel bowl via a peristaltic pump (Control Company, Friendswood, TX). Using this automated feeding system (similar to that described previously (Dilger and Johnson, 2010)), piglets received their daily allotted milk over 18 meals (once per hour). All animal experiments were in accordance with the National Institute of Health Guidelines for the Care and Use of Laboratory Animals and approved by the University of Illinois at Urbana–Champaign Institutional Animal Care and Use Committee.

### 2.2. Experimental design and treatments

Upon arrival, piglets were assigned to either the control group or the PRRSV infection group based on sex, litter of origin, and body weight. To determine the effect of early-life viral infection on neurogenesis and cell fate, on PD 7, 24 piglets (12 males and 12 females) were injected i.p. with BrdU (50 mg/kg, Sigma, St. Louis, MO, USA) and then inoculated intranasal with either 1 mL of $1 \times 10^5$ 50% tissue culture infected dose (TCID 50) of live PRRSV (strain P129-BV, obtained from the School of Veterinary Medicine at Purdue University, West Lafayette, IN, USA) or sterile phosphate buffered saline (PBS). Two PRRSV piglets developed diarrhea and were unable to complete the study. All remaining piglets (control male, $n = 6$; control female, $n = 6$; PRRSV male, $n = 5$; PRRSV female, $n = 5$) were sacrificed at PD 28. To determine the effect of early-life viral infection on hippocampal neuron morphology, a total of 16 piglets (8 males and 8 females) were inoculated with PRRSV or sterile PBS at PD 7. One PRRSV piglet developed diarrhea and was unable to complete the study. All remaining piglets were sacrificed at PD 31 (control male, $n = 4$; control, female $n = 4$; PRRSV male, $n = 4$; PRRSV female, $n = 3$). Animals were sacrificed around 4 weeks of age as the PRRSV infection has resolved as indicated by return to normal body temperature and sickness symptoms resolution (Fig. 1).

### 2.3. Assessment of infection

Daily body weights (kg) were obtained to monitor piglets' growth. In addition, daily rectal temperatures were obtained starting at PD 7. The willingness of the piglets to consume their first daily meal was determined starting at PD 7 using a feeding score (1 = no attempt to consume the milk; 2 = attempted to consume the milk, but did not finish within 1 min; 3 = consumed all of the milk within 1 min).

The presence of PRRSV antibodies in the serum of all piglets at the end of the study was analyzed by the Veterinary Diagnostic Laboratory (University of Illinois, Urbana, Illinois) using a PRRSV-specific ELISA kit (IDEXX Laboratories, Westbrook, ME, USA). This assay has 98.8% sensitivity and has a 99.9% specificity, with an S/P ratio of >0.4 indicating a positive sample. Serum TNF-α levels at the end of the study were determined using porcine-specific sandwich enzyme immunoassays (R&D Systems, Minneapolis, MN, USA).

### 2.4. Perfusions and tissue processing

For the neurogenesis and cell fate study, all animals were sacrificed and perfused at PD 28. A telazol:ketamine:xylazine solution was administered intramuscularly at 4.4 mg/kg BW (50.0 mg of tiletamine, plus 50.0 mg of zolazepam, reconstituted with 2.50 mL ketamine [100 g/L] and 2.50 mL xylazine [100 g/L]; Fort Dodge Animal Health, Fort Dodge, IA, USA). Eye blink and pain reflexes were tested to confirm deep anesthesia before piglets were perfused transcardially with phosphate buffered saline (PBS) and a 4% paraformaldehyde/PBS solution. Brains were extracted and post-fixed overnight. The hippocampus was removed and transferred to PBS with 30% sucrose until the tissue sank (~2 days). The entire hippocampus was sectioned using a cryostat into 40 μm sections in an axial plane from dorsal to ventral and collected into a 12-well plate. Six sections were collected into each well with a distance of 480 μm separating each well. As there is variation along the dorsal–ventral axis, tissue from the dorsal

region of the hippocampus was used for staining to maintain consistency.

### 2.5. BrdU-DAB

The DAB staining was adapted from previously described work (Kohman et al., 2012). Briefly, free floating sections were washed in Tris-buffering solution (TBS) and treated with 0.6% hydrogen peroxide solution for 30 min. Next, sections were placed in 50% deionized formamide for 90 min to denature DNA. Sections were then placed in a 10% 20× saline sodium citrate buffer for 15 min, 2 N hydrochloric acid for 30 min at 37 °C, and then 0.1 M boric acid (pH 8.5) for 10 min. After rinsing, sections were blocked with a solution of 0.3% Triton-X and 3% goat serum in TBS (TBS-X) for 30 min. The sections were then incubated with the primary antibody rat anti-BrdU (1:200; AbD Serotec, Raleigh, NC, USA) in TBS-X for 72 h at 4 °C. Sections were then rinsed with TBS, blocked with TBS-X for 30 min, and then incubated with a biotinylated goat anti-rat secondary antibody (1:250, Jackson ImmunoResearch Laboratories, West Grove, PA, USA) for 100 min. The ABC system (Vector, Burlingame, CA, USA) and diaminobenzidine kit (DAB; Sigma, St. Louis, MO, USA) were used for the chromogen.

### 2.6. Immunofluorescence

For the BrdU/NeuN double staining and the BrdU/GFAP/IBA-1 triple staining, a similar procedure was used as with DAB staining. The primary antibodies consisted of rat anti-BrdU (1:100; AbD Serotec, Raleigh, NC, USA), mouse anti-NeuN (1:50, Millipore, Temecula, CA, USA), mouse anti-GFAP (1:50, Santa Cruz Biotechnology, Santa Cruz, CA, USA), and rabbit anti-IBA1 (1:1000, Wako Chemicals, Richmond, VA, USA). All secondary fluorescent antibodies (All 1:250, Alexa-488, Cy3, and Alexa-647) were made in goat and incubated for 3 h at room temperature.

### 2.7. BrdU-DAB image analysis

Slides containing the DAB-stained tissue were digitized using a Nanozoomer digital pathology system at 20× magnification (Hamamatsu Photonics, Hamamatsu, Japan). The hippocampus of each tissue section was then exported at 10× resolution. Using ImageJ, regions of interest (ROI) were drawn for the suprapyramidal blade, infrapyramidal blade, and hilus of the dentate gyrus and ROI volumes measured. For the suprapyramidal and infrapyramidal blade, the granule cell layer and subgranular zone were included. An overview of the hippocampus with a highlighted view of the suprapyramidal blade can be seen in Fig. 2. ImageJ was used to automatically count the number of positively labeled cells in all three ROIs. The data are expressed as BrdU-positive cells per cubic micrometer. Thirty-two sections (~2400 positive cells) were used to validate the automated methods versus manual hand counting. Correlation analysis validated the automatic method with a slope no different from a 1-to-1 line and a Pearson $r$ value of 0.99. Unbiased estimation was used to correct for cells that could be intersecting with either the top or bottom of the tissue section. An average BrdU-positive nucleus was 6.5 μm in diameter (320 sampled), which is 16.25% of the 40 μm-thick section. BrdU-positive cell counts were multiplied by 0.8375 for unbiased estimation correction. These methods have been previously validated and published (Clark et al., 2008).

### 2.8. Immunofluorescence analysis

A Zeiss LSM 700 confocal microscope (20× objective) was used to acquire $z$-stack images with a 0.5 μm slice thickness in the dentate gyrus including the granule cell layer and subgranular zone. Images were deconvoluted using Autoquant (Media Cybernetics, Rockville, MD, USA). For the BrdU/NeuN co-localization, cells from both the suprapyramidal and infrapyramidal blades were acquired but later combined for analysis due to no differences between the two regions. Only cells from the suprapyramidal blade were sampled for the BrdU/GFAP/IBA-1 triple staining.

Raters blinded to the treatments manually counted the BrdU-positive and the number of either NeuN, GFAP, or IBA-1-positive cells that co-localized with BrdU-positive nuclei. A total of 2786 dentate gyrus BrdU-positive cells from 22 pigs were analyzed for co-localization. Two of the six sections per slide were randomly selected for analysis. Data is expressed as the proportion of BrdU-positive cells that co-localized with another cell marker.

### 2.9. Hippocampal neuronal architecture staining

To determine the effect of early-life viral infection on hippocampal neuron architecture, animals were euthanized at PD 31. A similar dose of TKX (see above) was used for induction of anesthesia and the animals were euthanized by intracardiac injection of sodium pentobarbital (86.0 mg/kg of B.W.; Fatal Plus®, Vortech Pharmaceuticals, Dearborn, MI, USA). The brain was removed and the left hippocampus was extracted and processed for Golgi–Cox staining as previously described (Jurgens et al., 2012; Richwine et al., 2008). Briefly, the left hippocampus was submerged in Golgi–Cox solution for 2 weeks at which point daily test slices were taken to track neuron filling. Tissues were removed after 4-weeks, dehydrated, and embedded in 12% celloidin. The dorsal hippocampus was sectioned at 140 μm and mounted on glass slides. Experimenters responsible for neuron tracing and spine density measurement were blinded to the treatments.

### 2.10. Neuron selection and tracing

Hippocampal neuron morphology was quantified using a Zeiss Axio Imager A.1 microscope and a computer-based system (Neurolucida; MBF Bioscience, Williston, VT, USA). NeuroExplorer (MBF Bioscience) was used for visualization and analysis of neuron tracings. Dentate granule cell neurons were selected from the suprapyramidal blade and were distinct from other neurons, not truncated, and were well filled. The granule cell neurons were traced at 40× magnification and then segments of the dendrites were captured at 100× magnification for dendritic spine analysis. Previous research has shown that the complexity of granule cells in the inner 2/3 of the granule cell layer (towards hilus) is different than cells in the outer 1/3 (towards molecular layer) (Green and Juraska, 1985). Therefore, 5 granule cell neurons from each region were traced and analyzed per pig. After tracing, an estimation of dendritic complexity was determined by calculating the total dendritic length and intersections. Dendritic tree morphology was analyzed using Sholl ring analysis. For the Sholl analysis, 3D concentric spheres with an increasing radius (20 μm increments) were placed around the cell body. The number of intersections of the dendrites and the concentric rings per radial distance from the soma were quantified.

### 2.11. Quantification of spine density and morphology

Spine density measurements were conducted on the same cells quantified for Sholl analysis. For each dentate gyrus granule cell, three dendritic segments were traced. Only 2–5° order branches and dendrites that were 20 μm or greater in length were selected. Each segment was at least 50 μm away from the cell soma. After neuron tracing was completed, dendritic spines were counted using Neurolucida. Spines were counted on both sides of the dendritic segment and classified according to their shapes; either thin, stubby, mushroom, filopodium, or branched (Tashiro and Yuste,

2003). The density of spines is expressed as number of spines per micron of dendrite.

### 2.12. Statistical analysis

Data analysis was conducted using the Proc MIXED procedure of SAS (SAS Institute Inc., Cary, NC, USA). Sickness measures were analyzed by two-way (*treatment* × *day*) repeated measures ANOVA with trial as a blocking factor, *day* as the within-subject measure, and *treatment* as the between subject measure. There were no significant differences due to sex, therefore it was not included in the final analysis of sickness symptoms. Neurogenesis data were analyzed by two-way (*treatment* × *sex*) ANOVA. Total dendritic length and total intersections in the inner and outer layer were analyzed separately by two-way (*treatment* × *sex*) ANOVA. Data from the Sholl analysis were analyzed by three-way (*treatment* × *sex* × *distance*) repeated measures ANOVA with *distance* as the within-subject measure, *treatment* and *sex* as the between subject measures, and with *pig* as a random effect and nested within *treatment* and *sex*. When a main effect or interaction was significant, *post hoc* Student's *t* tests using Fisher's least significant differences were used to identify significant pair-wise differences between means. Statistical significance was set at $p < 0.05$. Data are presented as means ± SEM.

## 3. Results

### 3.1. PRRSV infection and measures of sickness

Serum ELISA results indicated all control piglets were negative for PRRSV at the end of the study, whereas all piglets inoculated with PRRSV were positive for PRRSV. Body weight, rectal temperature, and the willingness to consume the first daily meal (feeding score) were determined to provide an indication of the sickness response of piglets infected with PRRSV (Fig. 1). Analysis of body weight data showed a significant effect of day ($F_{(30,962)} = 61.98$, $p < 0.001$) and a day × treatment interaction ($F_{(30,962)} = 2.25$, $p = 0.001$), where controls had higher weight gain toward the conclusion of the study. Overall, the effect of treatment on body weight was not significant ($F_{(1,34)} = 1.21$). Analysis of feeding score data revealed a significant effect of treatment ($F_{(1,34)} = 34.67$, $p < 0.001$), day ($F_{(24,734)} = 1.99$, $p = 0.003$), and a treatment × day interaction ($F_{(23,734)} = 2.08$, $p = .002$), indicating PRRSV piglets' motivation to consume the first meal of the day was reduced. Analysis of rectal temperature data showed a significant effect of treatment ($F_{(1,34)} = 80.15$), day ($F_{(24,766)} = 7.34$), and a treatment × day interaction ($F_{(24,766)} = 3.49$ (all, $p < 0.001$). PRRSV piglets became febrile 3 d after inoculation and remained so during most of the experimental period. At the conclusion of the study, plasma TNF-α concentration was significantly higher in PRRSV piglets (209.2 ± 36.3 pg/mL) compared to controls (21.5 ± 4.3 pg/mL) ($F_{(1,34)} = 32.97$ $p < 0.001$). Collectively, these data indicate infection with PRRSV in the neonatal period induced clinical signs of illness that persisted throughout the study period.

### 3.2. Hippocampal cell proliferation and survival

BrdU was injected at PD 7, just before PRRSV inoculation, and brain tissue was collected 3-wks later. Therefore, the number of BrdU+ cells represents the basal level of cell division at PD 7, subsequent division of cells labeled at PD 7, and the effects of viral infection on the survival of these labeled cells (Fig. 2). Analysis of BrdU+ cell density in the suprapyramidal blade revealed a

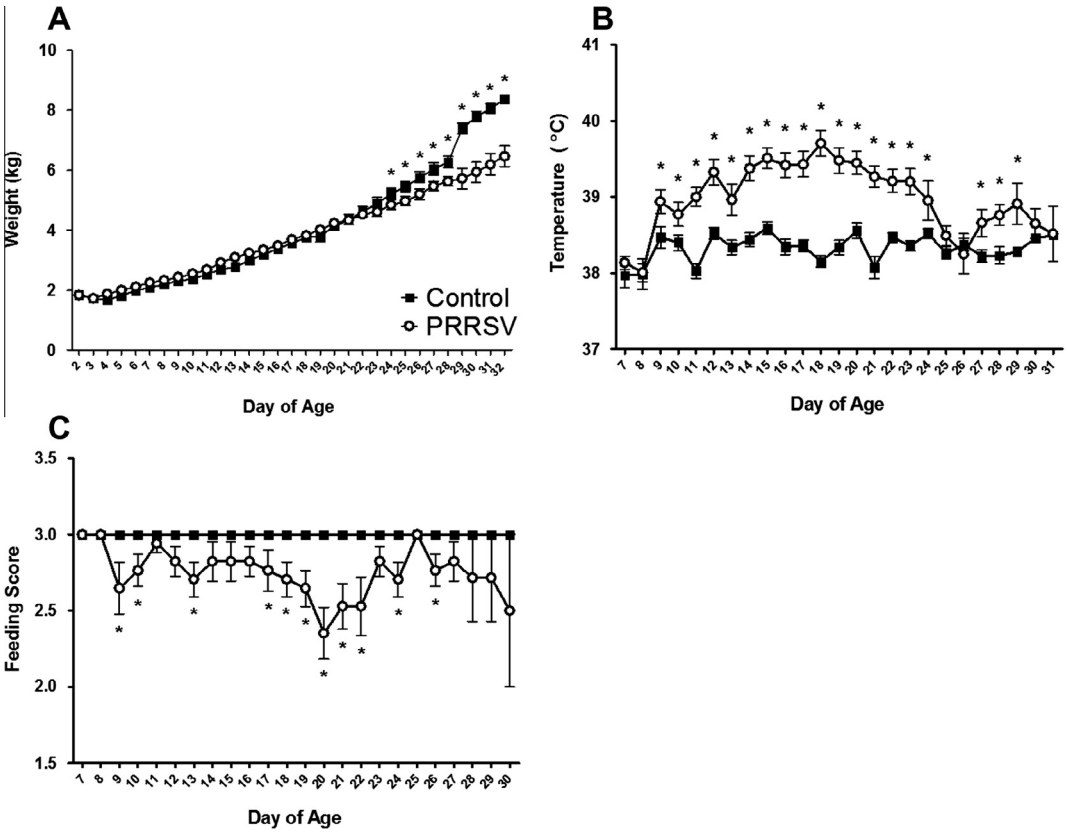


**Fig. 1.** (A–C) Daily recorded sickness measures. Body weight was recorded from the start of the experiment (A) and temperature (B) and feeding score (C) were measured starting prior to inoculation at 7 days of age. Data presented are means ± SEM (*$p < 0.05$ compared to controls).

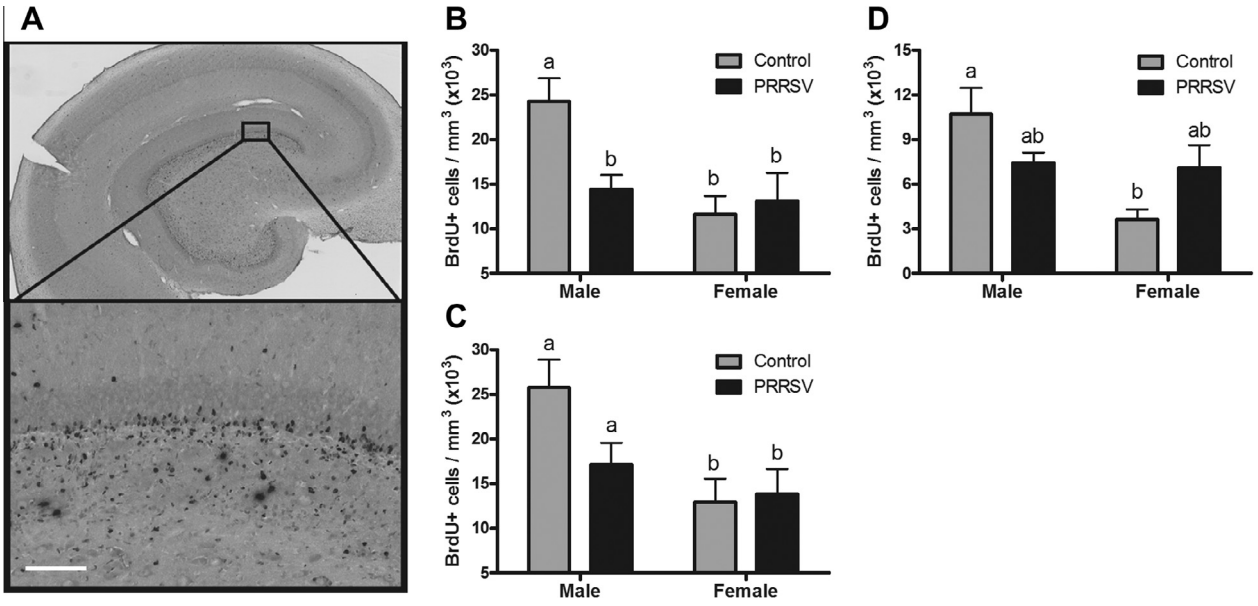


**Fig. 2.** (A) Representative section showing an overview of the hippocampus (top) with a magnified view of the suprapyramidal blade of the dentate gyrus (bottom). (B–D) Density of newly divided (BrdU+) cells in the suprapyramidal blade (A), infrapyramidal blade (B), and hilus (C) of the denate gyrus. Groups are separated by sex and treatment. Letters indicate the groups that were significantly different ($p < 0.05$). BrdU+ cells are indicated by DAB staining. Magnification = 2.5× (top), 20× (bottom); scale bar, 100 μm.

significant effect of sex ($F_{(1,18)} = 8.32, p = 0.01$) and a sex × treatment interaction ($F_{(1,18)} = 5.50$, $p = 0.03$), whereby control males had higher density of BrdU+ cells than control females (24,274 ± 2604 and 11,612 ± 2063 cells/mm$^3$, respectively, $p = 0.001$) and PRRSV caused a reduction of BrdU+ cells in males only (14,445 ± 1582 cells/mm$^3$, $p = 0.01$). In the infrapyramidal blade, only the effect of sex was significant ($F_{(1,17)} = 7.68$, $p = 0.01$). The density of BrdU+ cells in the hilus was also quantified. A significant effect of sex ($F_{(1,18)} = 8.04$, $p = 0.01$) and a sex × treatment interaction ($F_{(1,18)} = 6.8$, $p = 0.02$) was found, whereby female controls had a lower density of BrdU+ cells than male controls (3624 ± 678 and 10,691 ± 1786 cells/mm$^3$, respectively, $p = 0.001$) and whereas PRRSV numerically reduced the number of BrdU+ cells in males, it numerically increased the number of BrdU+ cells in females.

### 3.3. Cell fate

Immunofluorescence was used to determine the fate of BrdU+ cells in the dentate gyrus (Fig. 3). To estimate the percentage of Brdu+ cells that developed into mature neurons, the number of BrdU+ cells that co-labeled with NeuN was determined. Two-way ANOVA of the percentage of double-labeled cells revealed a significant effect of treatment ($F_{(1,18)} = 34.42$ $p < 0.001$) where in control piglets more than 80% of the cells labeled with BrdU at PD 7 differentiated into mature neurons by PD 28 but in PRRSV piglets only 57% of the cells labeled with BrdU at PD 7 differentiated into mature neurons. The marked reduction in neurogenesis caused by PRRSV was similar in both males and females. To estimate the percentage of BrdU+ cells that developed into microglia, the number of BrdU+ cells that co-labeled with IBA-1 was determined. Roughly 15% of the cells labeled with BrdU at PD 7 differentiated into microglia by PD 28 and this was not influenced by sex ($F_{(1,18)} = 1.05$), treatment ($F_{(1,18)} = 0.15$), or the sex × treatment interaction ($F_{(1,18)} = 0.21$). Tissue sections were also stained with GFAP in an attempt to quantify the number of BrdU+ cells that developed into astrocytes. However, due to the high density of astrocytes within the region analyzed and problems staining two intracellular markers, we were unable to clearly identify and quantify double labeled cells (data not shown).

### 3.4. Dendritic arborization

Total dendritic length and total intersections in the Sholl analysis were used to quantify the overall complexity of the inner and outer granule cell neurons (Fig. 4). A significant difference between the inner and outer granule cell neurons was evident ($F_{(1,22)} = 9.86$, $p = 0.0048$), therefore the two regions were analyzed separately for the overall complexity. Two-way ANOVA of the total dendritic length and the number of intersections of the inner dentate granule cell neurons showed neither an effect of sex, treatment or a sex × treatment interaction (all $p > 0.05$). However, there was a significant effect of sex on dendritic length ($F_{(1,11)} = 4.95, p = 0.048$) and number of intersections ($F_{(1,11)} = 5.99, p = 0.0328$) for neurons in the outer layer of the dentate gyrus where males had longer more complex dendrites than females. A similar trend was found when analyzing dendritic length and intersections within each Sholl interval. A repeated-measures ANOVA showed a significant effect of sex ($F_{(1,11)} = 5.95$, $p = 0.0328$) and distance from the soma ($F_{(16,176)} = 55.02$, $p < 0.0001$) on intersections for the outer dentate granule cell neurons. Males (2.11 ± 0.11) had more intersections than females (1.72 ± 0.12). Interestingly, analysis of the inner dentate granule cell neurons revealed a significant effect of distance ($F_{(17,187)} = 25.29, p < 0.0001$) and a distance × treatment interaction ($F_{(17,187)} = 2.26$, $p = 0.0041$). The altered dendritic arborization was due to shifting of the initial branching points away from the cell soma (within 40–140 μm) in the PRRSV piglets ($p < 0.05$).

### 3.5. Spine density

For the inner and outer portion of the granule cell layer spines were counted on both sides of the dendritic segment and classified according to their shape: thin, stubby, mushroom, filopodium, or branched (Figs. 5 and 6) Neither spine density or classification were affected in either the inner or outer granule cell layers by sex, treatment, or the sex × treatment interaction (all $p > 0.05$).

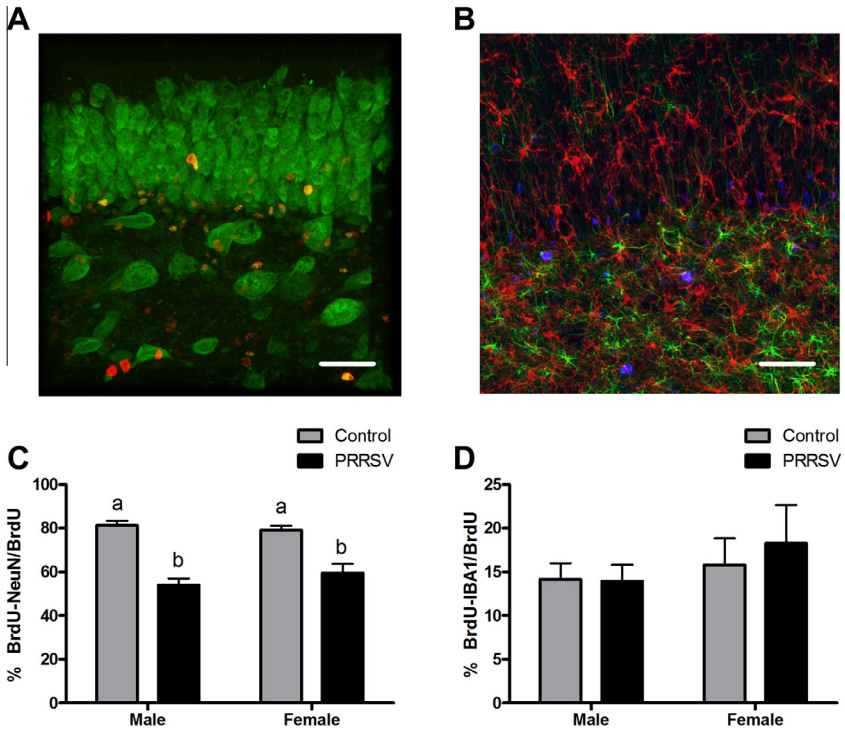


**Fig. 3.** (A–D) Representative maximum projection image sections showing double labeling (A) of antibodies against BrdU (new cell; red) and NeuN (mature neuron; green). Representative maximum projection image section showing triple labeling (B) with antibodies against BrdU (new cell; blue), Iba-1 (macrophage/microglia; red), and GFAP (astrocyte; green). The granule cell layer is located in the upper half of each photomicrograph. The proportion of newly divided cells that express NeuN (C) and IBA-1 (D) are plotted by sex and treatment. Means ± SEM are plotted with letters indicating differences between groups ($p < 0.05$). Magnification = 20×; scale bar = 50 μm. (For interpretation of the references to color in this figure legend, the reader is referred to the web version of this article.)

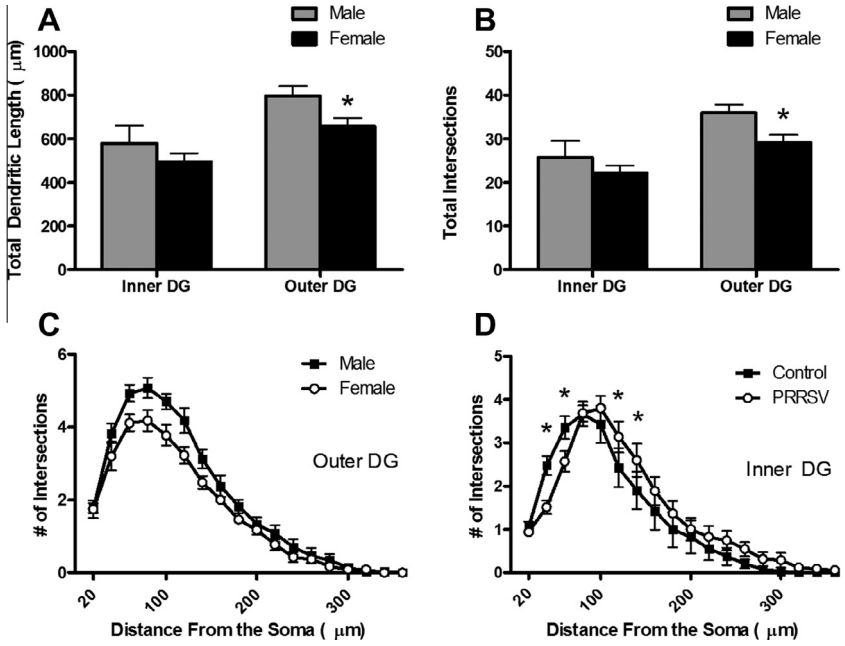


**Fig. 4.** (A–D) Females had reduced total dendritic length (A) and total intersections (B) in the outer dentate granule (DG) cell layer. Sholl analysis revealed that females had fewer intersections in the outer DG (C) and that PRRSV causes shifting of the first branching points away from the soma in the inner DG (D). Data are presented as means ± SEM (*$p < 0.05$ compared to controls).

## 4. Discussion

Respiratory infections during early-life are common, but knowledge of their impact on brain development is lacking. Due to ethical considerations and complications inherent to investigations in human neonates, progress in this area has been slow. Furthermore, the translation of data from rodent neurodevelopmental models to human infants is difficult due to substantial differences

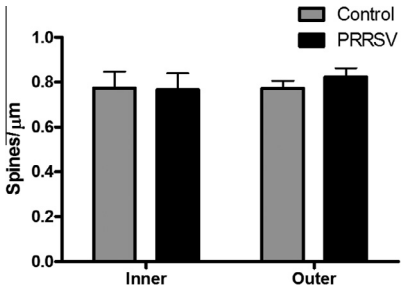


**Fig. 5.** PRRSV infection did not alter spine density of dendritic granule cells located in the inner or outer DG. Data are represented as means ± SEM.

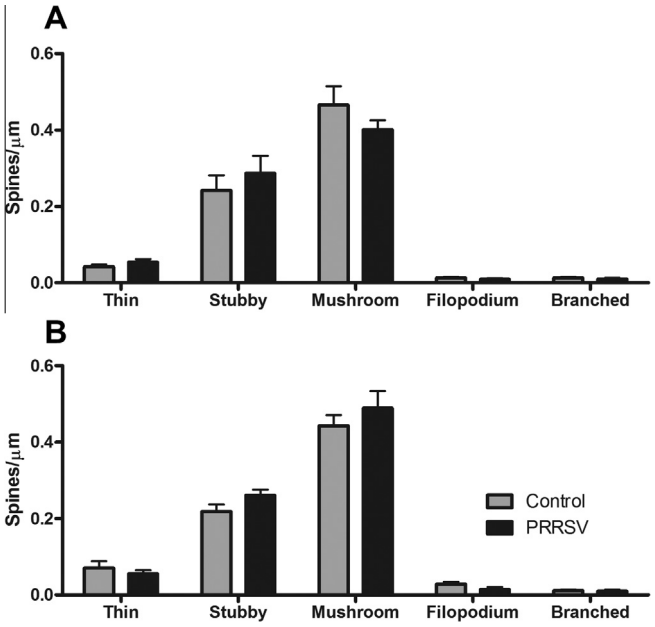


**Fig. 6.** PRRSV infection did not alter the distribution of spine morphology in the inner DG (A) or outer DG (B). Data are represented as means ± SEM.

in brain morphology and development. To overcome several obstacles, the current study was conducted using a highly tractable and translational piglet model (Elmore et al., 2014).

In young pigs PRRSV primarily infects and replicates in cells of the monocyte/macrophage lineage (Duan et al., 1997). PRRSV can activate microglia and cause production of pro-inflammatory cytokines in the brain either through immune-to-brain signaling pathways or by entering the CNS. In a recent study, several pro-inflammatory cytokines were elevated in serum 20 d after inoculation with PRRSV, and a number of pro-inflammatory genes, including interferon-γ, TNF-α, and IL-1β, were up regulated in several brain regions at the same time post inoculation (Elmore et al., 2014). Furthermore, the percentage of activated microglia, as indicated by expression of MHC class II, was markedly increased in piglets with PRRSV infection (Elmore et al., 2014). Microglial activation was positively correlated with fever, and negatively correlated with food motivation and learning and memory (Elmore et al., 2014). In the present study, piglets exhibited a sustained febrile response and increased circulating TNF-α at the conclusion of the experiment. This strongly suggests that PRRSV piglets had a sustained neuroinflammatory response throughout the study period.

Both *in vivo* and *in vitro* studies have shown that inflammation can lead to altered cell fate for newly divided cells. IL-1β causes a switch from neuronal to glial differentiation *in vitro* (Green et al., 2012). IL-1β can also inhibit the proliferation of neural progenitor cells and proliferation of newly born neurons (Green and Nolan, 2014). Similar to the *in vitro* data, prenatal and early postnatal immune activation in rodents causes a reduction in neuronal differentiation (Bland et al., 2010; Graciarena et al., 2010). Both increases and decreases in gliogenesis have been reported and may be time and insult dependent (Jarlestedt et al., 2013; Ratnayake et al., 2012). Here PRRSV infection was found to reduce the number of new cells differentiating into neurons by approximately 25% in both males and females (Fig. 3C). New neurons in the dentate have been shown to be necessary for hippocampal function including pattern separation and learning and memory (Deng et al., 2010; Villeda et al., 2011). Therefore, inhibition of neurogenesis in the neonatal period could underlie the infection-related deficits in spatial learning previously reported (Elmore et al., 2014). Whether the cognitive deficits persist beyond the active phase of the infection, is not known. The number of newly divided microglia cells was consistent across both sex and treatment at 15% of BrdU+ cells. There was a very high density of microglia in the subgranular zone and within the granule cell layer, but the absolute numbers were not quantified. We also stained for astrocytes using GFAP, but were unable to clearly identify BrdU+/GFAP+ cells. Astrocytes densely populated the subgranular zone and only had projections into the granule cell layer, but no cell bodies. The astrocytes were so dense that even with capturing *z*-stack image sets it was difficult to positively identify a BrdU+/GFAP+ cell and not rule out that two cells were in close proximity. Nonetheless, the data show that in healthy control piglets 80% of BrdU+ cells develop into neurons, and 15% into microglia. This leaves only 5% undetermined. In piglets infected with PRRSV, however, only 55% of the BrdU+ cells develop into neurons, and 15% into microglia. This leaves 30% of the BrdU+ cells unidentified. The undetermined cells could be astrocytes, oligodendrocytes, or undifferentiated cells.

Research with adult rodents has shown that peripheral immune activation can reduce the survival of new neurons in the dentate gyrus (Ekdahl et al., 2003). The majority of neurogenesis studies in adult rodents have used males only. As many developmental disorders have a higher incidence in one sex or the other, it is important to study both males and females. Here we find that there is a sexual dimorphism in the number of surviving BrdU+ cells in the dentate gyrus with males having more surviving cells than females. This dimorphism is also seen in the dentate gyrus and CA1 region of the neonatal rat (Bowers et al., 2010; Zhang et al., 2008). PRRSV infection caused a significant reduction of surviving cells in males, but did not affect females. This suggests that either females are not as susceptible to inflammation or there is a protective mechanism to combat these signals. Alternatively, at postnatal day 4, male rats have significantly more microglia in the dentate gyrus than females which could lead to sex differences in the inflammatory response (Schwarz et al., 2012). Studies in rodents have used both acute inflammatory stimuli, such as LPS, or systemic infection with *Escherichia coli* in male mice during the early postnatal period (Bland et al., 2010; Jarlestedt et al., 2013). These studies show reductions in new cell survival in the dentate gyrus, consistent with what we found in male piglets with a chronic viral infection. The earlier studies in rodents did not include females.

In addition to neurogenesis, changes in hippocampal neuron morphology were assessed. Dentate granule cells were characterized as they have been shown to be sensitive to inflammatory insult (Jurgens et al., 2012). The soma location within the granule cell layer may be associated with "age" of the neuron as new cells are born in the subgranular zone and migrate into the inner granule cell layer (Mongiat and Schinder, 2011). Although we did not specifically test for cell age, the microenvironment may be different for the inner granule cell neurons and inflammation may affect

them differently (Mongiat and Schinder, 2011). PRRSV infection caused a shifting in the shape of the inner granule cell dendritic tree, extending the primary dendrite length before the first branching points. These results are dissimilar to adult influenza studies which found that inflammation in adulthood caused a retraction of dendrites (Jurgens et al., 2012). The reason for the extension of the primary dendrite is not clear. The highest density of microglia was found in the subgranular zone, so it may be that the inner granule layer cells are exposed to a higher pro-inflammatory cytokine load. Additionally, studies have found that size of the dentate increases with prenatal inflammation, so it is possible that the primary dendrite must travel through more cells before starting to branch (Golan et al., 2005).

Additionally, results showed that there was a sexual dimorphism in the complexity of outer dentate granule cell neurons, but the shape of the dendritic tree was similar among males and females. This difference is similar to rodents where males have more complex outer dentate granule cell neurons (Juraska et al., 1985). We also found that the outer dentate granule cell neurons were more complex than the inner neurons, also similar to rodents (Green and Juraska, 1985). Although no differences were found in dendritic spine density, the distribution of spine morphology is noteworthy. During early development, stubby spines are dominant with some filopodia (Nimchinsky et al., 2002). As synaptic connections are made and strengthened, the spine takes on a more mature mushroom morphology (Bourne and Harris, 2008). Our data illustrate that the most abundant morphology was stubby and mushroom spines, a similar trend to the postnatal distribution in rodents (Harris et al., 1992).

In conclusion, inflammation during early-life has the potential to cause short- and long-term disruptions in brain development. Our data indicate that neonatal respiratory infection can reduce cell survival, change cell fate, and can alter hippocampal cell morphology in a sexually dimorphic manor. The conclusions of this study are limited as changes were only quantified at one end point. The PRRSV piglets were almost symptomatically recovered at this time. Tracking long-term changes would be useful to see if early life infection permanently impacts development or if these changes are reversed with time. Additional work is needed to characterize the unidentified BrdU+ cells. Regardless of these limitations, we show that early-life respiratory infection can impact brain development. Further work with this model will allow for testing of therapeutic strategies to modulate the neuroimmune response with aims of preventing adverse developmental outcomes.

## Conflicts of interest

The authors declare no conflicts of interest.

## Acknowledgments

This work was supported by NIH HD069899. We thank Dr. Janice M. Juraska (Department of Psychology, University of Illinois Urbana–Champaign) for helping with the neuron morphology analysis. Additionally, we thank Sarah Main, Tara Garcia, Joshua Doppelt, Emmanuelle Asrow, Brandi Burton, and Emily Solan for their assistance in this project.

## References

Bland, S.T., Beckley, J.T., Young, S., Tsang, V., Watkins, L.R., Maier, S.F., Bilbo, S.D., 2010. Enduring consequences of early-life infection on glial and neural cell genesis within cognitive regions of the brain. Brain Behav. Immun. 24, 329–338.

Boksa, P., 2010. Effects of prenatal infection on brain development and behavior: a review of findings from animal models. Brain Behav. Immun. 24, 881–897.

Bourne, J.N., Harris, K.M., 2008. Balancing structure and function at hippocampal dendritic spines. Annu. Rev. Neurosci. 31, 47–67.

Bowers, J.M., Waddell, J., McCarthy, M.M., 2010. A developmental sex difference in hippocampal neurogenesis is mediated by endogenous oestradiol. Biol. Sex Differences 1, 8.

Cacci, E., Ajmone-Cat, M.A., Anelli, T., Biagioni, S., Minghetti, L., 2008. In vitro neuronal and glial differentiation from embryonic or adult neural precursor cells are differently affected by chronic or acute activation of microglia. Glia 56, 412–425.

Clark, P.J., Brzezinska, W.J., Thomas, M.W., Ryzhenko, N.A., Toshkov, S.A., Rhodes, J.S., 2008. Intact neurogenesis is required for benefits of exercise on spatial memory but not motor performance or contextual fear conditioning in C57BL/6J mice. Neuroscience 155, 1048–1058.

Conrad, M.S., Dilger, R.N., Johnson, R.W., 2012. Brain growth of the domestic pig (*Sus scrofa*) from 2 to 24 weeks of age: a longitudinal MRI study. Dev. Neurosci. 34, 291–298.

Dantzer, R., Kelley, K.W., 2007. Twenty years of research on cytokine-induced sickness behavior. Brain Behav. Immun. 21, 153–160.

Deng, W., Aimone, J.B., Gage, F.H., 2010. New neurons and new memories: how does adult hippocampal neurogenesis affect learning and memory? Nat. Rev. Neurosci. 11, 339–350.

Dietrich, R.B., Bradley, W.G., Zaragoza, E.J., Otto, R.J., Taira, R.K., Wilson, G.H., Kangarloo, H., 1988. MR evaluation of early myelination patterns in normal and developmentally delayed infants. Am. J. Roentgenol. 150, 889–896.

Dilger, R.N., Johnson, R.W., 2010. Behavioral assessment of cognitive function using a translational neonatal piglet model. Brain Behav. Immun. 24, 1156–1165.

Duan, X., Nauwynck, H.J., Pensaert, M.B., 1997. Virus quantification and identification of cellular targets in the lungs and lymphoid tissues of pigs at different time intervals after inoculation with porcine reproductive and respiratory syndrome virus (PRRSV). Vet. Microbiol. 56, 9–19.

Ekdahl, C.T., 2012. Microglial activation – tuning and pruning adult neurogenesis. Front. Pharmacol. 3.

Ekdahl, C.T., Claasen, J.-H., Bonde, S., Kokaia, Z., Lindvall, O., 2003. Inflammation is detrimental for neurogenesis in adult brain. Proc. Natl. Acad. Sci. U.S.A. 100, 13632–13637.

Elmore, M.R., Burton, M.D., Conrad, M.S., Rytych, J.L., Van Alstine, W.G., Johnson, R.W., 2014. Respiratory viral infection in neonatal piglets causes marked microglia activation in the hippocampus and deficits in spatial learning. J. Neurosci. 34, 2120–2129.

Elmore, M.R., Dilger, R.N., Johnson, R.W., 2012. Place and direction learning in a spatial T-maze task by neonatal piglets. Anim. Cogn. 15, 667–676.

Golan, H.M., Lev, V., Hallak, M., Sorokin, Y., Huleihel, M., 2005. Specific neurodevelopmental damage in mice offspring following maternal inflammation during pregnancy. Neuropharmacology 48, 903–917.

Graciarena, M., Depino, A.M., Pitossi, F.J., 2010. Prenatal inflammation impairs adult neurogenesis and memory related behavior through persistent hippocampal TGFβ1 downregulation. Brain Behav. Immun. 24, 1301–1309.

Green, E.J., Juraska, J.M., 1985. The dendritic morphology of hippocampal dentate granule cells varies with their position in the granule cell layer: a quantitative Golgi study. Exp. Brain Res. 59, 582–586.

Green, H.F., Nolan, Y.M., 2014. Inflammation and the developing brain: consequences for hippocampal neurogenesis and behavior. Neurosci. Biobehav. Rev. 40, 20–34.

Green, H.F., Treacy, E., Keohane, A.K., Sullivan, A.M., O'Keeffe, G.W., Nolan, Y.M., 2012. A role for interleukin-1beta in determining the lineage fate of embryonic rat hippocampal neural precursor cells. Mol. Cell. Neurosci. 49, 311–321.

Hall, C.B., Weinberg, G.A., Iwane, M.K., Blumkin, A.K., Edwards, K.M., Staat, M.A., Auinger, P., Griffin, M.R., Poehling, K.A., Erdman, D., Grijalva, C.G., Zhu, Y., Szilagyi, P., 2009. The burden of respiratory syncytial virus infection in young children. N. Engl. J. Med. 360, 588–598.

Harris, K.M., Jensen, F.E., Tsao, B., 1992. Three-dimensional structure of dendritic spines and synapses in rat hippocampus (CA1) at postnatal day 15 and adult ages: implications for the maturation of synaptic physiology and long-term potentiation. J. Neurosci. 12, 2685–2705.

Huttenlocher, P.R., 1979. Synaptic density in human frontal cortex – developmental changes and effects of aging. Brain Res. 163, 195–205.

Jarlestedt, K., Naylor, A.S., Dean, J., Hagberg, H., Mallard, C., 2013. Decreased survival of newborn neurons in the dorsal hippocampus after neonatal LPS exposure in mice. Neuroscience 253, 21–28.

Juraska, J.M., Fitch, J.M., Henderson, C., Rivers, N., 1985. Sex differences in the dendritic branching of dentate granule cells following differential experience. Brain Res. 333, 73–80.

Jurgens, H.A., Amancherla, K., Johnson, R.W., 2012. Influenza infection induces neuroinflammation, alters hippocampal neuron morphology, and impairs cognition in adult mice. J. Neurosci. 32, 3958–3968.

Kelley, K.W., Bluthé, R.-M., Dantzer, R., Zhou, J.-H., Shen, W.-H., Johnson, R.W., Broussard, S.R., 2003. Cytokine-induced sickness behavior. Brain Behav. Immun. 17, 112–118.

Kohman, R.A., DeYoung, E.K., Bhattacharya, T.K., Peterson, L.N., Rhodes, J.S., 2012. Wheel running attenuates microglia proliferation and increases expression of a proneurogenic phenotype in the hippocampus of aged mice. Brain Behav. Immun.

Lynch, M.A., 2002. Interleukin-1 beta exerts a myriad of effects in the brain and in particular in the hippocampus: analysis of some of these actions. Vitam. Horm. 64, 185–219.

Meyer, U., Feldon, J., Dammann, O., 2011. Schizophrenia and autism: both shared and disorder-specific pathogenesis via perinatal inflammation? Pediatr. Res. 69, 26R–33R.

Milatovic, D., Zaja-Milatovic, S., Montine, K.S., Horner, P.J., Montine, T.J., 2003. Pharmacologic suppression of neuronal oxidative damage and dendritic degeneration following direct activation of glial innate immunity in mouse cerebrum. J. Neurochem. 87, 1518–1526.

Mongiat, L.A., Schinder, A.F., 2011. Adult neurogenesis and the plasticity of the dentate gyrus network. Eur. J. Neurosci. 33, 1055–1061.

Nimchinsky, E.A., Sabatini, B.L., Svoboda, K., 2002. Structure and function of dendritic spines. Annu. Rev. Physiol. 64, 313–353.

Ratnayake, U., Quinn, T.A., Castillo-Melendez, M., Dickinson, H., Walker, D.W., 2012. Behaviour and hippocampus-specific changes in spiny mouse neonates after treatment of the mother with the viral-mimetic poly I: C at mid-pregnancy. Brain Behav. Immun. 26, 1288–1299.

Rice, D., Barone Jr., S., 2000. Critical periods of vulnerability for the developing nervous system: evidence from humans and animal models. Environ. Health Perspect. 108 (Suppl. 3), 511–533.

Richwine, A.F., Parkin, A.O., Buchanan, J.B., Chen, J., Markham, J.A., Juraska, J.M., Johnson, R.W., 2008. Architectural changes to CA1 pyramidal neurons in adult and aged mice after peripheral immune stimulation. Psychoneuroendocrinology 33, 1369–1377.

Schwarz, J.M., Sholar, P.W., Bilbo, S.D., 2012. Sex differences in microglial colonization of the developing rat brain. J. Neurochem. 120, 948–963.

Tashiro, A., Yuste, R., 2003. Structure and molecular organization of dendritic spines. Histol. Histopathol. 18, 617–634.

Tong, L., Balazs, R., Soiampornkul, R., Thangnipon, W., Cotman, C.W., 2008. Interleukin-1 beta impairs brain derived neurotrophic factor-induced signal transduction. Neurobiol. Aging 29, 1380–1393.

Vallieres, L., Campbell, I.L., Gage, F.H., Sawchenko, P.E., 2002. Reduced hippocampal neurogenesis in adult transgenic mice with chronic astrocytic production of interleukin-6. J. Neurosci. 22, 486–492.

Villeda, S.A., Luo, J., Mosher, K.I., Zou, B., Britschgi, M., Bieri, G., Stan, T.M., Fainberg, N., Ding, Z., Eggel, A., Lucin, K.M., Czirr, E., Park, J.S., Couillard-Despres, S., Aigner, L., Li, G., Peskind, E.R., Kaye, J.A., Quinn, J.F., Galasko, D.R., Xie, X.S., Rando, T.A., Wyss-Coray, T., 2011. The ageing systemic milieu negatively regulates neurogenesis and cognitive function. Nature 477, 90–94.

Wu, M.D., Hein, A.M., Moravan, M.J., Shaftel, S.S., Olschowka, J.A., O'Banion, M.K., 2012. Adult murine hippocampal neurogenesis is inhibited by sustained IL-1beta and not rescued by voluntary running. Brain Behav. Immun. 26, 292–300.

Wu, M.D., Montgomery, S.L., Rivera-Escalera, F., Olschowka, J.A., O'Banion, M.K., 2013. Sustained IL-1β expression impairs adult hippocampal neurogenesis independent of IL-1 signaling in nestin+ neural precursor cells. Brain Behav. Immun. 32, 9–18.

Zhang, J.M., Konkle, A.T., Zup, S.L., McCarthy, M.M., 2008. Impact of sex and hormones on new cells in the developing rat hippocampus: a novel source of sex dimorphism? Eur. J. Neurosci. 27, 791–800.